Magnetic Blind Beamforming for Battery-Free Wireless Sensor Networks

Albert A. Ofori, *Student Member, IEEE,* and Hongzhi Guo, *Member, IEEE*

***Abstract*—It is challenging to maintain a large number of wireless sensors in inaccessible media, such as underground and intra-body. Tiny battery-free sensors are desirable since they create negligible impacts on the environment and do not require battery replacement. Battery-free sensors can harvest energy from wireless signals to support their normal operation. However, they cannot cooperate with the charger due to the lack of energy in the initial stages. This paper proposes the Magnetic Blind Beamforming (MagBB) using tri-axis coils to power up battery-free wireless sensors. Battery-free sensors with randomly orientated coils may experience significant misalignment losses and they may not receive any energy from the charger. MagBB uses a set of optimized current vectors to generate rotating magnetic fields which can ensure that coils with arbitrary orientations can receive sufficient voltages for charging. It does not require any information about the battery-free sensor's coil orientation or location. A proof-of-concept prototype is developed. The numerical simulations and experimental results show that MagBB can efficiently improve the reliability of wireless charging. Sensor coils with arbitrary orientation and location within the operation range can harvest sufficient energy. This technology has the potential of powering ultra-dense wireless sensors with low communication overhead.**

***Index Terms*—Battery-free sensors, blind beamforming, tri-axis coils, underground wireless sensors, wireless charging.**

I. Introduction

Wireless sensors play an important role in precision agriculture by collecting information such as light intensity and leaf color. More recently, underground wireless sensors are introduced to precision agriculture to monitor soil nutrition and moisture [2], [3]. Today's wireless sensors are bulky and expensive, which are not suitable for large-scale wireless sensor networks. Hence, wireless sensors are used sparsely on farms. As sensor technology improves, sensors can be made smaller and less intrusive, thereby making them more suitable for in-situ sensing [4], [5]. However, battery usually determines the lifetime of a wireless sensor, which requires periodical replacement or recharging. The inaccessible media, such as soil, make this task challenging. For instance, an underground sensor would require precise knowledge of the sensor location to dig it out for battery replacement. To avoid this labor-intensive task, tiny battery-free sensors are desirable. For example, battery-free sensors can be deployed aboveground and underground to monitor various parameters regarding plant health [6], as shown in Fig. 1. Since these sensors are small and low-cost, they do not require precise deployment, which is more convenient compared with traditional sensors. More importantly, they do not require battery replacement which significantly reduces the cost of maintenance.

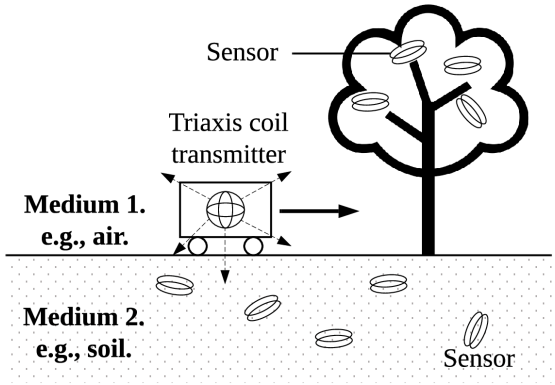

Fig. 1: A mobile robot is used to charge multiple battery-free sensors with tiny unidirectional coils. The robot is equipped with a tri-axis coil.

Battery-free sensors rely on ambient energy harvesting or wireless energy transfer to support their normal operation. The ambient energy harvesting may causes significant delay in data transmission due to unreliable energy sources [7]. On the contrary, active wireless energy transfer is more reliable at the cost of high power consumption. As shown in Fig. 1, a mobile robot is used to wirelessly power up and communicate with battery-free sensors. Sensors can harvest energy, then sense and send data to the robot. Since sensors are randomly located surrounding a plant, their orientations and locations are unknown. Also, plant growth is a dynamic process; previous information of sensor locations and orientations may not be useful. Existing wireless energy transfer using magnetic MIMO systems relies on channel estimation to optimally design transmit signals in order to efficiently charge sensors [8]–[11]. Channel estimation, however, is only ideal for active sensors which can provide channel information feedback to the charger.

Wireless charging for battery-free sensors in inhomogeneous media is challenging due to the following reasons:

- **Threshold voltage.** Typical energy harvesting circuits use a full-wave bridge rectifier [5] which consists of diodes to convert the induced AC voltages to DC voltages. Since diodes have a threshold voltage V_{th}, lower than which the circuit cannot harvest any energy. The typical V_{th} is above 200 mV which is hard to obtain when

This material is based upon work supported by the National Science Foundation under Grant No. CNS1947748 and HRD1953460.

A short version of this paper was presented in IEEE 18th Annual Consumer Communications & Networking Conference (CCNC) in Jan. 2021 [1].

The authors are with the Engineering Department, Norfolk State University, Norfolk, VA, USA. Emails: a.a.ofori@spartans.nsu.edu and hguo@nsu.edu.

the distance between a charger and a sensor is large. Moreover, considering the tiny size of the battery-free sensor, the antenna is not efficient in receiving energy due to its low profile.

- **Unknown coil/receiver information.** Since a battery-free sensor does not store any energy, it cannot perform channel estimation for wireless energy transfer. Without the channel state information, efficient beamforming cannot be implemented. Thus, the wireless charger has no information about the receiver and traditional magnetic beamforming fails in such a system.
- **Random coil/receiver location and orientation.** In an uncontrolled and relatively dynamic environment, the location of a sensor might change, or its antenna orientation in space might be altered by various factors. Even though sensors may be placed at specific, documented locations in the soil, the potentially dynamic nature of the underground environment can alter the exact location of a sensor over time. The growth of plants and the consequent penetration of their roots into the soil, for instance, have the potential to displace underground sensors to a unpredictable degree. Moreover, other uncontrollable phenomena such as erosion and seasonal changes in moisture can result in remarkable variations in communication channel conditions.
- **Inhomogeneous media.** The wireless signal propagation is hard to predict due to the inhomogeneous environment, which may require complex beamforming algorithms. However, it is not trivial to map the environment and predict signal propagation.

In this paper, we use magnetic-based wireless charging to power randomly located and orientated battery-free sensors [8], [9]. Magnetic signals in the near-field can efficiently penetrate through the soil-air boundary which experience negligible reflection losses [12]. In the near-field, we can almost consider the environment as a homogeneous medium. The mobile charger employs a tri-axis coil with three mutually perpendicular unidirectional coils. By optimally controlling the currents in the tri-axis coil, we can create magnetic fields in any direction. We design the Magnetic Blind Beamforming (MagBB) algorithm to rotate the magnetic fields at a certain point to ensure that an arbitrarily orientated coil can receive sufficient voltage to power the battery-free sensor. MagBB does not require any channel state information which is suitable for battery-free sensors. MagBB signals can be added constructively at the receiver to improve the charging efficiency. The impacts of distance, orientation and the number of beamforming current vectors are analytically studied. We also design a proof-of-concept prototype to demonstrate the benefits of the proposed approach using off-the-shelf components.

The main contributions of this paper include:

- We develop the MagBB algorithm. Since it does not require channel state information, MagBB has the potential to extend the existing wireless charging range to power battery-free sensors. To the best of our knowledge, this is the first work that investigates tri-axis coil-based blind beamforming.

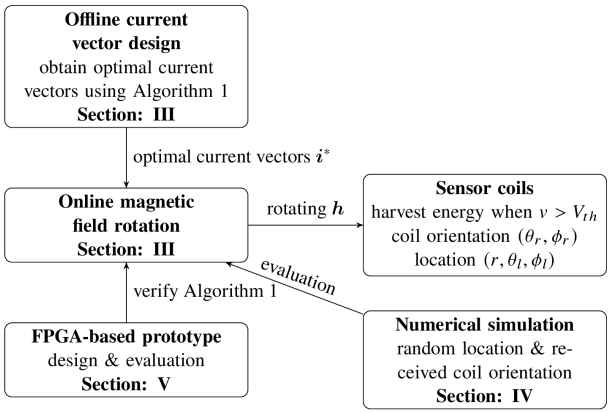

Fig. 2: Illustration of the structure of this paper.

- We provide analytical analysis on the impact of distance and the number of beamforming current vectors, which provide an insightful understanding of the benefits and limitations of the proposed approach.
- We design a proof-of-concept prototype using off-the-shelf components to validate the proposed approach.
- Although the considered application in this paper is precision agriculture, this technology has the potential of being used for wireless sensing in many other inhomogeneous media and wireless charging for ultra-dense Internet of Things.

The rest of this paper is organized as follows and a block diagram showing the structure of this paper is given in Fig. 2. The background and related work are introduced in Section II. The MagBB algorithm is developed and analyzed in Section III. After that, the numerical analyses are given in Section IV. The proof-of-concept prototype is designed and evaluated in Section V. Finally, this paper is concluded in Section VI.

II. Related Work

Wireless charging plays an important role in green Internet of Things (IoT) [13], through which we can efficiently power a large number of IoT devices, including wireless sensors. Since devices may be placed randomly, the received power is heterogeneous. To address this issue, various solutions have been proposed, including mobile chargers [14], quasistatic cavity resonance [15], and relays [16]. Among these solutions, the RFID-based battery-free sensors and the magnetic-based wireless charging are closely related to this paper.

The threshold voltage problem also arises in existing RFID-based wireless sensing systems. The threshold voltage of the energy harvester limits the operation range of RFID. In [5], signals with multiple frequencies are transmitted to create a multipath fading effect, which can align signals constructively or destructively at the receiver. It is a kind of blind beamforming approach since it does not require any channel state information from the receiver. If signals are aligned constructively, it may overcome the threshold voltage issue and power the RFID. However, in the near-field of magnetic coils, the multipath fading is negligible and there is almost no phase shift. Thus, the blind beamforming proposed for Ultra-High Frequency (UHF) RFID cannot be directly adopted.

In [12], [17], magnetic coils have been used for underground wireless communication. It mainly demonstrates two advantages. First, HF (3 MHz to 30 MHz) signals can penetrate through the soil-air interface efficiently. The 13.56 MHz band is evaluated in [12] on a farm which demonstrates a reliable channel. Second, HF signals generate less interference since they have a high falloff rate. Wireless charging requires high transmission power. The UHF signals can generate significant interference for existing wireless services.

More importantly, wireless charging using multiple magnetic coils has been widely accepted and used in consumer electronics. In [8], [10], magnetic MIMO system is designed and improved, which can provide a high charging efficiency for multiple wireless devices. This idea has been extended to many important works [9], [11], [18]–[22].

The above magnetic beamforming algorithms are developed for battery-powered electronic devices, which can cooperate with the charger to provide channel state information. However, battery-free sensors cannot respond without being powered up [23]. Existing NFC (Near Field Communication) sensors require a short communication range (around 10 cm) to receive sufficient power for operation. As the distance increases, the performance is limited by coil orientation and the threshold voltage of the energy harvester. In [24], a magnetic blind beamforming algorithm is proposed using a planar coil array. Although it aims to solve a similar problem, the algorithm is fundamentally different from our approach. Also, the planar array occupies a larger 2D space. The blind beamforming algorithm tries to power up all the sensors with arbitrary orientation. This is related to the fair charging problem in terrestrial wireless power transfer for multiple devices [25], [26]. However, existing works mainly aim to fairly allocate power, while this paper focus on overcome the threshold voltage problem for arbitrarily orientated coils.

We use a 3D tri-axis coil that can be carried by a mobile robot to charge battery-free sensors. The tri-axis coil is widely used as a magnetic sensor for localization and orientation sensing. It has also been adopted for wireless underground communication [27]–[29] and wireless underwater communication [30], [31]. Existing works rely on the knowledge of wireless channels to optimally design the transmit signals, while we do not have the information in this paper.

III. Magnetic Blind Beamforming

In this section, we introduce the tri-axis coil model first. Then, we design MagBB by rotating coil current vectors. After that, we provide analytical analysis of the proposed algorithm and compare it with low-complexity solutions.

Since we use long-wavelength magnetic signals, in the following we neglect the inhomogeneity of the environment and consider the sensors are located in the air. Also, due to the limited space of a battery-free sensor, it can only use a tiny unidirectional coil as the antenna and its orientation and location are unknown for the mobile robot. The mobile robot is equipped with a larger tri-axis coil antenna. Some key mathematical notations are given in Table I.

TABLE I: Mathematical Notation

Symbol	Description
a_t	the radius of transmit coil
a_r	the radius of receive coil
P_{max}	the maximum transmission power
V_{th}	the threshold voltage of the harvester circuit
n_{cv}	the number of current vectors
(θ_r, ϕ_r)	receive coil's orientation in Spherical Coordinate System
(r, θ_l, ϕ_l)	receive coil's location in Spherical Coordinate System
$\boldsymbol{u}$	receive coil's orientation in Cartesian Coordinate System
$\boldsymbol{h}$	magnetic field at the receiver
$\boldsymbol{i}$	tri-axis coil current vector
N_t and N_r	transmit coil and receive coil number of turns, respectively
r_t and r_r	transmit coil and receive coil resistance, respectively

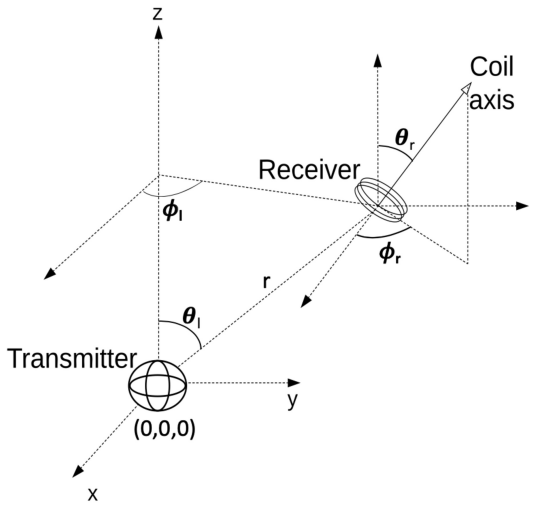

Fig. 3: Illustration of the angular parameters used to describe the location (θ_l, ϕ_l) and orientation (θ_r, ϕ_r) of the receiver coil relative to the transmitter.

A. Tri-Axis Coil Array

The generated magnetic fields can be aligned in any direction in the 3D space based on the value of current that is fed into individual unidirectional coils. The current can be varied to produce a rotating magnetic field that would be varied in fixed steps with a period to provide sufficient magnetic fields to any sensor in a given direction to overcome its threshold voltage. The tri-axis coil, as shown in Fig. 3, has three unidirectional coils with each coil axis aligned along each of the Cartesian axis (i.e., x, y, and z).

We define pseudo-axes for a unidirectional coil using a unit vector $\boldsymbol{n} = [x_n, y_n, z_n]^T$, where $(\cdot)^T$ is the transpose of a vector or matrix. Since the coil size is much smaller than the wavelength, we consider the coil as a magnetic dipole, and the dipole moment has the same direction as $\boldsymbol{n}$. The tri-axis coil can be considered as an array of three magnetic dipoles with directions $\boldsymbol{N} = [\boldsymbol{n}_1, \boldsymbol{n}_2, \boldsymbol{n}_3]$ [30]. Let the currents supplied to coils with axes aligned along the x_n, y_n and z_n axis be i_1, i_2 and i_3, respectively. We assume the coils are identical and have the same radius $a_1 = a_2 = a_3 = a_t$ and number of turns $N_1 = N_2 = N_3 = N_t$.

Since the aim is to achieve direction control by changing the currents, we can use one variable $\boldsymbol{i} \in \mathbb{C}^3$ to denote coil currents, i.e., $\boldsymbol{i} = [i_1, i_2, i_3]^T$. Then, the beamforming problem simplifies to the problem of obtaining optimal $\boldsymbol{i}$. To achieve this in a simplified manner, we introduce variables C_r, C_θ,

$C_\phi \in \mathbb{C}$ such that:

$$\boldsymbol{C} = \begin{bmatrix} C_r \\ C_\theta \\ C_\phi \end{bmatrix} = \begin{bmatrix} \frac{jka_t^2 N_t}{2r^2} \cdot [1 + \frac{1}{jkr}] \cdot e^{-jkr} \\ \frac{k^2 a_t^2 N_t}{4r} \cdot [1 + \frac{1}{jkr} - \frac{1}{(kr)^2}] \cdot e^{-jkr} \\ \frac{k^2 a_t^2 N_t}{4r} \cdot [1 + \frac{1}{jkr} - \frac{1}{(kr)^2}] \cdot e^{-jkr} \end{bmatrix} \quad (1)$$

where $j = \sqrt{-1}$, k is the propagation constant, and r is the distance between the transmitter and the receiver. Then, the magnetic fields generated by a tri-axis coil at a point with spherical coordinates (r, θ_l, ϕ_l) relative to the transmitter can be represented in a Spherical Coordinates System (SCS) as

$$\boldsymbol{h}_r = [h_{rr}, h_{r\theta}, h_{r\phi}]^T = \boldsymbol{C} \cdot \boldsymbol{\Gamma} \cdot \boldsymbol{i} \quad (2)$$

where

$$\boldsymbol{C} = \begin{bmatrix} C_r & 0 & 0 \\ 0 & C_\theta & 0 \\ 0 & 0 & C_\phi \end{bmatrix} \quad (3)$$

and

$$\boldsymbol{\Gamma} = \begin{bmatrix} \sin\theta_l \cos\phi_l & \sin\theta_l \sin\phi_l & \cos\theta_l \\ \cos\theta_l \cos\phi_l & \cos\theta_l \sin\phi_l & -\sin\theta_l \\ -\sin\phi_l & \cos\phi_l & 0 \end{bmatrix}, \quad (4)$$

where θ_l and ϕ_l are the angle parameters that are used to describe the location of the observation point, as shown in Fig. 3. The above equations can be obtained from [32] and [33] using spherical coordinates rotation. Here, $\boldsymbol{C}$ is a function of distance, coil parameters and environmental parameters, and $\boldsymbol{\Gamma}$ is a function of the observation point location in the 3D space. For example, if receivers are on a sphere with the transmitter with a tri-axis coil in the center, they have the same $\boldsymbol{C}$ but different $\boldsymbol{\Gamma}$.

Magnetic field $\boldsymbol{h}_r$ is obtained in a SCS, while the coil orientation is described in a Cartesian Coordinates System (CCS). By using the following equation, we can obtain $\boldsymbol{h}$ in a CCS,

$$\boldsymbol{h} = \boldsymbol{T} \cdot \boldsymbol{h_r}, \quad (5)$$

where

$$\boldsymbol{T} = \begin{bmatrix} \sin\theta_l \cos\phi_l & \cos\theta_l \cos\phi_l & -\sin\phi_l \\ \sin\theta_l \sin\phi_l & \cos\theta_l \sin\phi_l & \cos\phi_l \\ \cos\theta_l & -\sin\theta_l & 0 \end{bmatrix}. \quad (6)$$

The aim is to produce an optimal magnetic field in the intended direction of observation and align the magnetic field vector in the direction of a unit vector along the axis of a receive coil at the observation point. We define the orientation of the receive coil as a unit vector $\boldsymbol{u} \in \mathbb{R}^3$ such that:

$$\boldsymbol{u} = [\sin\theta_r \cos\phi_r, \sin\theta_r \sin\phi_r, \cos\theta_r]^T, \quad (7)$$

where θ_r and ϕ_r describe the orientation of the receiver coil axis, as shown in Fig. 3. To find three optimal current values can be complex. This problem can be modeled as an optimization problem that aims to reduce the difference between the received magnetic field direction and the orientation of the receive coil.

We define a power threshold P_{max} which should not be exceeded in supplying power to the transmit unidirectional coils. We define a diagonal matrix $\boldsymbol{R} \in \mathbb{R}^{3\times3}$ representing the resistances of the transmit unidirectional coil, where r_x is the resistance of transmitter coil x and $r_1 = r_2 = r_3 = r_t$ such that:

$$\boldsymbol{R} = \begin{bmatrix} r_t & 0 & 0 \\ 0 & r_t & 0 \\ 0 & 0 & r_t \end{bmatrix}. \quad (8)$$

The resultant magnetic field $\boldsymbol{h}_r$ should also induce a voltage that is large enough to overcome the threshold voltage in the receiver energy harvesting circuit. The induced voltage v can be expressed as:

$$v = -\omega\mu_r\mu_0 N_r \pi a_r^2 \boldsymbol{u}^T \cdot \boldsymbol{h}, \quad (9)$$

where μ_r is the relative permeability of the medium and μ_0 is the permeability of vacuum, N_r is the number of turns of receive coil and a_r is the radius of receive coil.

B. Magnetic Blind Beamforming

To efficiently charge battery-free sensors, we need to maximize the induced voltage given limited transmission power. If we have the knowledge of the receiver's coil orientation $\boldsymbol{u}$, this problem can be efficiently solved by optimizing the transmit current to reduce the misalignment loss between $\boldsymbol{h}$ and $\boldsymbol{u}$. However, without the knowledge of $\boldsymbol{u}$ nor the mutual inductance, we cannot obtain the optimal transmit current. Also, different from terrestrial electromagnetic wave-based multiple antenna systems, equally allocate transmission power is not suboptimal in this paper, which will result in unreliable performance, as will be shown in our numerical analysis.

To overcome the threshold voltage and efficiently charge coils with arbitrary orientations, we use MagBB and the main idea is shown in Fig. 4. First, when we use constant currents for tri-axis coils, the generated magnetic field always points to one direction. Different from electromagnetic wave-based wireless communication/charging in the terrestrial environments, magnetic-based wireless communication/charging operates in the near-field with a short distance, where the multipath fading can be neglected. As shown in the upper of Fig. 4a, if the magnetic field direction is parallel with the receiver's coil axis, the received power can be maximized. However, if the magnetic field direction is perpendicular to the receiver's coil axis, no voltage can be induced. Thus, the performance of using constant currents for the tri-axis coil is highly random, which is not predictable nor reliable without the knowledge of $\boldsymbol{u}$.

MagBB is based on current vector rotation. As shown in Fig. 4b, 5 current vectors are used to create 5 magnetic fields with different directions (their magnitudes may also be different). For example, if we use 60 seconds to charge a sensor, each current vector is allocated with 12 seconds. Since the 5 vectors cover 180 degrees, we can ensure that coils with arbitrary orientations can be covered and at least one current vector can induce voltage that is larger than the threshold voltage to charge a sensor. Next, we try to study the following three problems: 1) how to design the current vectors? 2) how many current vectors do we need? and 3) does the current vector depend on the receiver's location?

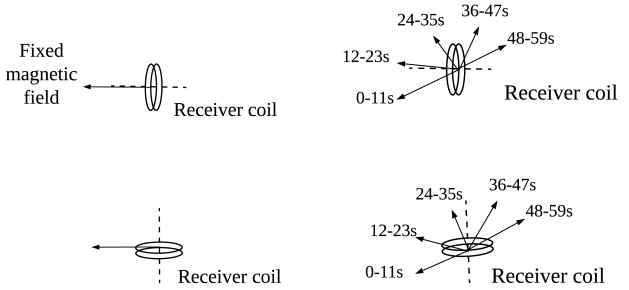

(a) Constant transmitter current supply to charge randomly oriented coils

(b) Transmitter current set rotating magnetic field through space.

Fig. 4: Illustration of constant and rotating magnetic fields for different receiver coil orientations. (a) two instances where maximum voltage is induced when coil axis is aligned with magnetic field (top) and zero voltage induced when coil axis is perpendicular to magnetic field (bottom); (b) induced voltage in the receiver coil by the rotating magnetic field at some points during the charging cycle is independent of coil orientation.

1) Current Vector Design: Since we rotate the magnetic field direction at the receiver, we need the location information of the receiver to obtain the current vectors. Next, we first consider a specific location (r, θ_l, ϕ_l), then we prove that the results are independent of the receiver's location. We create n_{cv} current vectors to rotate the magnetic field direction to cover a hemisphere. The following problem is formulated to obtain the current vector $\boldsymbol{i}$,

$$\text{(P1): } \underset{\boldsymbol{i}\in\mathbb{C}^3}{\text{minimize}} \left\| \boldsymbol{u} - \frac{\boldsymbol{h}}{\parallel \boldsymbol{h} \parallel} \right\|^2 \tag{10}$$

$$s.t. \quad \boldsymbol{i}^H \boldsymbol{R} i \leq 2P_{max}; \tag{11}$$

$$|\boldsymbol{u}^T \boldsymbol{h}| > \frac{V_{th}}{\omega \mu_r \mu_0 N_r \pi a_r^2}, \tag{12}$$

where $(\cdot)^H$ is the hermitian and $\boldsymbol{u}$ is the targeting magnetic field direction. The objective function aims to design the magnetic field direction to point to the receive coil orientation $\boldsymbol{u}$. The first constraint is due to the transmission power and the second constraint ensures that the induced voltage is larger than the rectifier's threshold voltage V_{th}. Consider the targeting magnetic field directions as $\{\boldsymbol{u}_l, l = 1, \cdots, n_{cv}\}$. By substituting $\{\boldsymbol{u}_l, l = 1, \cdots, n_{cv}\}$ into the above problem, we can obtain the associated current vectors. We uniformly sample points on a unit hemisphere (radius is 1) to obtain unit vectors $\{\boldsymbol{u}_l, l = 1, \cdots, n_{cv}\}$ (the vectors point from the origin to the points on the hemisphere). Since ideally the received voltages have the same magnitude but opposite phase if the incident magnetic fields have opposite directions, we only use a hemisphere to reduce current vector correlations, as well as the computation complexity.

However, directly solving (P1) is challenging. In order to homogenize this optimization problem, a slack variable $t \in \mathbb{R}$ is introduced such that:

$$t = \parallel \boldsymbol{h} \parallel \text{ and } t^2 = \boldsymbol{i}^H \cdot \tilde{\boldsymbol{C}}^H \cdot \tilde{\boldsymbol{C}} \cdot \boldsymbol{i}. \tag{13}$$

where $\tilde{\boldsymbol{C}} = \boldsymbol{C}\boldsymbol{\Gamma}$. Since the change of coordinate system does not affect the magnitude of the magnetic fields, we have $\|\boldsymbol{h}_r\| = \|\boldsymbol{h}\|$.

The optimization problem can be updated as

$$\text{(P2): } \underset{\boldsymbol{i}\in\mathbb{C}^3}{\text{minimize}} \parallel t\boldsymbol{u} - \boldsymbol{h} \parallel^2 \tag{14}$$

$$s.t. \ \boldsymbol{i}^H \tilde{\boldsymbol{C}}^H \tilde{\boldsymbol{C}} \boldsymbol{i} = t^2 \tag{15}$$

$$\boldsymbol{i}^H \boldsymbol{R} \boldsymbol{i} \leq 2P_{max} \tag{16}$$

$$\boldsymbol{i}^H \tilde{\boldsymbol{C}}^H \boldsymbol{u}\boldsymbol{u}^T \tilde{\boldsymbol{C}} \boldsymbol{i} > \frac{V_{th}^2}{\omega^2 (\mu_r \mu_0 N_r \pi a_r^2)^2} \tag{17}$$

which can subsequently be solved using the method of Semidefinite Relaxation [34].

Our ability to use Semidefinite Relaxation is incumbent on the ability to express our problem in the form $\boldsymbol{x}^H \boldsymbol{A} \boldsymbol{x}$ where $\boldsymbol{x} \in \mathbb{C}^N$ is the variable or system of variables to be optimized and $\boldsymbol{A} \in \mathbb{C}^{N \times N}$ is a function or group of functions with known values that constitute a positive semidefinite matrix. Since the value of $\boldsymbol{i}$ could be complex in nature, the optimization problem can be expressed as a real value equation whereby we decompose all potentially complex values into their real and imaginary forms such that:

$$\hat{\boldsymbol{u}} = \begin{bmatrix} \Re\{\boldsymbol{u}\} \\ \Im\{\boldsymbol{u}\} \end{bmatrix}, \quad \hat{\boldsymbol{i}} = \begin{bmatrix} \Re\{\boldsymbol{i}\} \\ \Im\{\boldsymbol{i}\} \end{bmatrix}, \tag{18}$$

$$\hat{\boldsymbol{C}} = \begin{bmatrix} \Re\{\tilde{\boldsymbol{C}}\} & -\Im\{\tilde{\boldsymbol{C}}\} \\ \Im\{\tilde{\boldsymbol{C}}\} & \Re\{\tilde{\boldsymbol{C}}\} \end{bmatrix}, \tag{19}$$

$$\hat{\boldsymbol{R}} = \begin{bmatrix} \Re\{\boldsymbol{R}\} & -\Im\{\boldsymbol{R}\} \\ \Im\{\boldsymbol{R}\} & \Re\{\boldsymbol{R}\} \end{bmatrix}. \tag{20}$$

This decomposition essentially doubles all dimensions such that any matrix $\boldsymbol{X} \in \mathbb{C}^{N \times N}$ becomes $\hat{\boldsymbol{X}} \in \mathbb{R}^{2N \times 2N}$ and all vectors $\boldsymbol{x} \in \mathbb{C}^N$ become $\hat{\boldsymbol{x}} \in \mathbb{R}^{2N}$, i.e., $\boldsymbol{u}$ and $\boldsymbol{i}$ become 6×1 matrices and $\tilde{\boldsymbol{C}}$ becomes a 6×6 matrix. The homogenized objective function $\parallel t\boldsymbol{u} - \boldsymbol{h} \parallel^2$ can then be accurately written as:

$$\begin{bmatrix} \hat{\boldsymbol{i}}^T & t \end{bmatrix} \boldsymbol{A} \begin{bmatrix} \hat{\boldsymbol{i}} \\ t \end{bmatrix} = \begin{bmatrix} \hat{\boldsymbol{i}}^T & t \end{bmatrix} \begin{bmatrix} \hat{\boldsymbol{C}}^T \hat{\boldsymbol{C}} & -\hat{\boldsymbol{C}}^T \boldsymbol{u} \\ -\hat{\boldsymbol{u}}^T \hat{\boldsymbol{C}} & \parallel \hat{\boldsymbol{u}} \parallel^2 \end{bmatrix} \begin{bmatrix} \hat{\boldsymbol{i}} \\ t \end{bmatrix}. \tag{21}$$

In this form, we can adequately apply semidefinite programming in solving this problem. We can express a single variable $\boldsymbol{\beta} \in \mathbb{R}^{7 \times 7}$ as the product of our variable matrix and its transpose:

$$\begin{bmatrix} \hat{\boldsymbol{i}} \\ t \end{bmatrix} \begin{bmatrix} \hat{\boldsymbol{i}}^T & t \end{bmatrix} = \boldsymbol{\beta}. \tag{22}$$

The MATLAB code based on the objective function and constraints is given in Algorithm 1, which is solved using CVX toolbox [35], [36]. We use $\boldsymbol{X}(i, j)$ to denote the element in the ith row and jth column of $\boldsymbol{X}$ and $\boldsymbol{x}(i : j)$ to denote the ith to jth elements in a vector $\boldsymbol{x}$.

The approximated solution is a rank-1 matrix $\boldsymbol{\beta}$ and to obtain the approximated $\boldsymbol{i}$ we use the dominant eigenvector:

$$\boldsymbol{\beta} \approx \lambda_{max} \boldsymbol{q}\boldsymbol{q}^T, \tag{23}$$

where $\lambda_{max} \in \mathbb{R}$ is the largest eigenvalue of matrix $\boldsymbol{\beta}$ and $\boldsymbol{q} \in \mathbb{R}^{N \times 1}$ is the eigenvector associated with λ_{max}. The eigenvector that is associated with the largest eigenvalue of

Algorithm 1: Optimal Current Vector

Input: $\boldsymbol{A}$ (Equ. (21)), $\hat{\boldsymbol{R}}$ (Equ. (20)), P_{max}, $\hat{\boldsymbol{C}}$ (Equ. (19)), $\boldsymbol{u}$, V_{th}, ω, μ_r, μ_0, N, a
Output: $\boldsymbol{\beta}$
cvx_begin
variable $\boldsymbol{\beta}$(7,7) symmetric;
minimize($trace(\boldsymbol{A}\boldsymbol{\beta})$);
subject to
$trace(\hat{\boldsymbol{R}} \cdot \boldsymbol{\beta}(1{:}6,1{:}6)) \leq 2P_{max}$;
$trace(\hat{\boldsymbol{C}}^T\hat{\boldsymbol{C}} \cdot \boldsymbol{\beta}(1{:}6,1{:}6)) = \boldsymbol{\beta}(7,7)$;
$trace((\hat{\boldsymbol{C}}^T\boldsymbol{u}\boldsymbol{u}^T\hat{\boldsymbol{C}}) \cdot \boldsymbol{\beta}(1{:}6,1{:}6)) \geq \frac{V_{th}^2}{\omega^2(\mu_r\mu_0 N\pi a^2)^2}$;
$\boldsymbol{\beta}$ ==semidefinite(7);
cvx_end

$\boldsymbol{\beta}$ is considered as the solution $\boldsymbol{i}$. From this approximation, the optimal decomposed current vector can be obtained as $\boldsymbol{i}^\star \in \mathbb{R}^{7\times 1}$ such that:

$$\boldsymbol{i}^\star = \sqrt{\lambda_{max}} \cdot \boldsymbol{q}, \tag{24}$$

with

$$\begin{bmatrix} \Re\{\boldsymbol{i}_1\} \\ \Re\{\boldsymbol{i}_2\} \\ \Re\{\boldsymbol{i}_3\} \end{bmatrix} = \boldsymbol{i}^\star(1:3); \quad \begin{bmatrix} \Im\{\boldsymbol{i}_1\} \\ \Im\{\boldsymbol{i}_2\} \\ \Im\{\boldsymbol{i}_3\} \end{bmatrix} = \boldsymbol{i}^\star(4:6). \tag{25}$$

The performance of a given set of currents is then obtained by finding the optimum current for a coil in a given location and in all possible directions of orientation. The efficacy of this system lies in its ability to induce a voltage in a randomly oriented coil at a given location for a sufficiently long period such that the induced voltage $v > V_{th}$. Note that, the optimization problem may not have a solution if the threshold voltage is large or the transmission power is small. There is a limitation on the charging range.

Semidefinite Relaxation has a worst complexity of $O(max\{m,n\}^4 n^{1/2}\log(1/\epsilon_a))$, where m is the number of constraints, n is the row number of $\boldsymbol{\beta}$, and ϵ_a is the approximation accuracy [34]. The complexity is obtained by counting the arithmetic operations of an interior-point method, which has been well-studied in [37], [38]. In this paper, we have $m = 3$ and $n = 7$. The original problem is quadratically constrained quadratic programing which is hard to solve. Semidefinite Relaxation demonstrates a good approximation which is close to 1; ϵ_a depends on the specific problem. Thus, in this paper, the complexity is $O(\log(1/\epsilon_a))$ to solve a single Semidefinite Relaxation problem. Since we have n_{cv} current vectors and for each of them we need to solve a Semidefinite Relaxation problem, the overall complexity is $O(n_{cv}\log(1/\epsilon_a))$.

2) Received Energy: The performance of wireless charging is evaluated using power transfer efficiency in most existing works [8], [9]. However, the power transfer efficiency cannot evaluate MagBB's performance. MagBB uses a set of current vectors, and it is guaranteed that some of them are efficient and some are not. The wireless power transfer efficiency is highly random for a randomly orientated and located coil. Instead, we use the received energy within a period. Battery-free sensors accumulate energy using a capacitor and wake up when the energy is above a threshold. The objective of using MagBB is to ensure that all the sensors can harvest sufficient energy to power up. Thus, it is more reasonable to use received energy. For the n_{cv} current vectors, we cycle through them periodically to ensure that sensors can be periodically charged to support their normal operation. Consider the period as T_c; we divide it into n_{cv} time slots with each being ΔT. During each time slot, the received voltage is v_i. Then, the overall harvested energy is

$$E_v = \sum_{i=1}^{n_{cv}} \mathbb{1}(v_i > V_{th}) \frac{v_i^2}{2r_r}\Delta T, \tag{26}$$

where r_r is the receiver resistance and $\mathbb{1}(\cdot)$ is an indicator function which is 1 if the condition is satisfied. The voltage drop across the energy harvester is neglected in this paper.

3) Number of Current Vectors: There is a tradeoff between the charging efficiency and the charging time interval of ΔT. On one hand, if n_{cv} is large, with high probability, we can obtain the optimal (or nearly optimal) current vector to charge the receiver with near-zero misalignment loss. On the other hand, a large n_{cv} reduces ΔT since T_c is a constant. Even if the charging efficiency is high, a small ΔT may reduce the overall received energy.

Since the receiver's orientation $\boldsymbol{u}$ is an arbitrary vector in 3D space, to fully capture all possibilities, we need three current vectors in minimum. Otherwise, if $n_{cv} < 3$, there are some points that cannot capture any voltage due to misalignment losses. On the contrary, there is no limitation on the maximum number of current vectors since with more current vectors, we can cover more orientations. However, as the number increases, the complexity of the algorithms increases, and the correlation between two adjacent current vectors increases, which may waste resources.

The minimum number of current vectors can be designed in the following way. First, we define three random vectors $\boldsymbol{v_1}, \boldsymbol{v_2}, \boldsymbol{v_3} \in \mathbb{R}^{3\times 1}$ for the magnetic field direction based on which we derive orthogonal basis $\boldsymbol{u_1}, \boldsymbol{u_2}, \boldsymbol{u_3} \in \mathbb{R}^{3\times 1}$ using Gram–Schmidt process such that:

$$\boldsymbol{u_1} = \boldsymbol{v_1} \tag{27}$$

$$\boldsymbol{u_2} = \boldsymbol{v_2} - \frac{\boldsymbol{v_2}\cdot\boldsymbol{u_1}}{\|\boldsymbol{u_1}\|^2}\boldsymbol{u_1} \tag{28}$$

$$\boldsymbol{u_3} = \boldsymbol{v_3} - \frac{\boldsymbol{v_3}\cdot\boldsymbol{u_1}}{\|\boldsymbol{u_1}\|^2}\boldsymbol{u_1} - \frac{\boldsymbol{v_3}\cdot\boldsymbol{u_2}}{\|\boldsymbol{u_2}\|^2}\boldsymbol{u_2} \tag{29}$$

By normalizing $\boldsymbol{u_1}$, $\boldsymbol{u}_2$, and $\boldsymbol{u}_3$, we obtain the orthonormal basis $\boldsymbol{e_1}, \boldsymbol{e_2}, \boldsymbol{e_3} \in \mathbb{R}^{3\times 1}$ which represent three mutually orthogonal coil directions such that:

$$\boldsymbol{e}_n = \frac{\boldsymbol{u_n}}{\|\boldsymbol{u_n}\|} \tag{30}$$

Knowledge of these orientations can then be used in finding the optimum currents for a coil aligned along these directions by substituting into (10).

4) Variance of Received Energy: If we only use three beamforming vectors, the received energy has a large variance, i.e., some sensors receive high energy if they are more aligned with the beamforming vectors, otherwise, the received energy

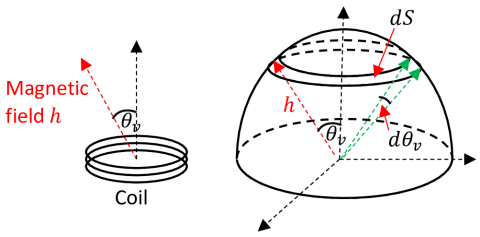

Fig. 5: Illustration of magnetic field direction and its distribution on a hemisphere.

is low. A large variance means the received energy for some sensors may be extremely small that cannot support their normal functions. As the number of beamforming vectors increases, the received energy of sensors becomes similar since all the sensors can obtain a nearly aligned beamforming vector. However, since the overall charging time is a constant, the more beamforming vectors we use, the shorter the charging time for each beamforming vector, i.e., $\Delta T = T_c/n_{cv}$. Thus, there is a tradeoff between the variance of received energy of all the sensors and the number of beamforming vectors.

Next, we obtain an analytical relation between the number of beamforming vectors and the received energy. We consider $n_{cv} \geq 3$ to ensure that the minimum requirement can be met. As shown in Fig. 5, assume the magnitudes of magnetic fields are homogeneous, which are considered as h in the sequel. Then, the received power is proportional to $(h\cos\theta_v)^2$ and the received energy with a single beamforming vector is

$$E_v(\theta_v) \propto \frac{T_c(h\cos\theta_v)^2}{n_{cv}},\ \theta_v \leq \theta_t, \tag{31}$$

where θ_t is due to the threshold voltage, i.e., if the angle is larger than a threshold, $\cos\theta_v$ is small and the energy harvester cannot receive any energy. When n_{cv} is large, the beamforming vectors point to points uniformly distributed on the hemisphere. Assume the hemisphere's radius is 1. The probability that the angle between the magnetic field and the coil axis being θ_v is

$$P(\theta_v) = \frac{dS}{2\pi} = \sin\theta_v d\theta_v, \tag{32}$$

where $d\theta_v$ is an infinitesimal angle as shown in Fig. 5. For a single beamforming vector, the mean received energy is

$$\mathbb{E}(E_v(\theta_v)) = \int_0^{\theta_t} P(\theta_v)E_v(\theta_v)d\theta_v \propto \frac{T_c h^2}{3n_{cv}}(1-\cos^3\theta_t). \tag{33}$$

and the variance is

$$Var(E_v(\theta_v)) = \mathbb{E}[(E_v(\theta_v) - \mathbb{E}(E_v(\theta_v)))^2] \propto \frac{T_c^2 h^4}{n_{cv}^2} C_{ang}, \tag{34}$$

where $C_{ang} = \left[\frac{1}{5}(1-\cos^5\theta_t) - \frac{1}{9}(1+\cos\theta_t)(1-\cos^3\theta_t)^2\right]$. $E_v(\theta_v)$ is obtained using (31) and $\mathbb{E}(E_v(\theta_v))$ is obtained using (33). Then, we calculate the expected value with respect to the variable θ_v. Thus, with all the n_{cv} beamforming vectors, the mean received energy is

$$\mathbb{E}(E_r) \propto \frac{T_c h^2}{3}(1-\cos^3\theta_t). \tag{35}$$

and the variance is

$$Var(E_r) \propto \frac{T_c^2 h^4}{n_{cv}} C_{ang}. \tag{36}$$

The above equations suggest that the mean received energy is independent of the number beamforming vector. However, a large n_{cv} can reduce the variance of E_r to ensure that all the sensor receives similar energy.

5) Receiver Location Dependency: Note that, we optimize the current vectors at one specific location. Next, we explore how the location of a receiver coil affects the magnetic field intensity, and how to maximize this field. From (2), we introduce the scalar and angular coefficients of the equation. It can be seen that $\boldsymbol{\Gamma}$ is an orthogonal matrix since $\boldsymbol{\Gamma}\boldsymbol{\Gamma}^T = \boldsymbol{\Gamma}^T\boldsymbol{\Gamma} = \boldsymbol{I}$. The angular coefficient, therefore, does not affect the magnitude of the generated magnetic field vector. The factor affecting the efficacy of a given current vector set in any location would, therefore, depend principally on the scalar coefficient $\boldsymbol{C}$. From (1), it can be seen that $C_\theta = C_\phi$. Also, it can be seen, quite intuitively, that the scalar coefficient magnitudes are inversely proportional to r. In the near-field of coil antenna ($r \ll$ wavelength$/2\pi$),

$$C_r \approx 2C_\theta \approx 2C_\phi. \tag{37}$$

The induced voltage is proportional to $\boldsymbol{h}_r$ which is given in (2). Since $\boldsymbol{\Gamma}$ is an orthogonal matrix, $\boldsymbol{h}_r$ is equivalent to the result of projecting $\boldsymbol{i}$ in a new orthogonal coordinates system using $\boldsymbol{\Gamma}$ and then scale the three elements using C_r, C_θ, and C_ϕ. Given the distance, C_r, C_θ, and C_ϕ do not change on the sphere. In the near-field, due to (37), $\boldsymbol{h}_r$ are similar, which does not depend on the location on the sphere. Assuming the applied current is at its maximum accepted value such that $\|\boldsymbol{i}\|^2_{\max} = \frac{2P_{\max}}{r_t}$, then $C_\theta\|\boldsymbol{i}\|_{\max} \leq \|\boldsymbol{h}\| \leq C_r\|\boldsymbol{i}\|_{\max}$ and this stands true for the near-field region. This relatively low variation in magnetic field intensity as the receiver location changes for a constant current is very convenient for reliable charging of a receiving sensor.

However, as we venture into the far-field ($kr >> 1$) [32], the scalar coefficient values start to diminish such that $C_r << C_\theta = C_\phi$. In this case, the projected $\boldsymbol{i}$ is scaled unevenly. If the projected vector has a dominant element and it is scaled by C_r, the $\boldsymbol{h}_r$ can be extremely small. The magnitude of the magnetic field can, therefore, vary widely as the receiver location changes, potentially resulting in erratic charging efficiency as the produced voltage can drop below the desired value with a slight change in the relative location of the receiver to the transmitter. This makes a far-field application of this implementation relatively unreliable.

From the above discussion, we learn that despite the beamforming vectors are optimized at a specific receiving location, they can be used to efficiently charge sensors at any location in the near-field with any orientation. This approach may have dramatically different performance in the far-field due to the inhomogeneity of magnetic fields. However, in the far-field, the long distance prevents the receiver from capturing strong signals. Existing magnetic-based wireless charging does not work in the far-field. Also, note that, instead of optimizing the beamforming vectors at a given receiving location, we can

TABLE II: Simulation Parameters

Symbol	Value	Symbol	Value
μ_r	1	f	13.56 MHz
ϵ_o	8.85×10^{-12} F/m	ϵ_r	1.0006
a_t	0.1 m	a_r	0.01 m
$P_{\max}$	50 W	V_{th}	0.2 V
r_t	1 Ω	r_r	0.2 Ω

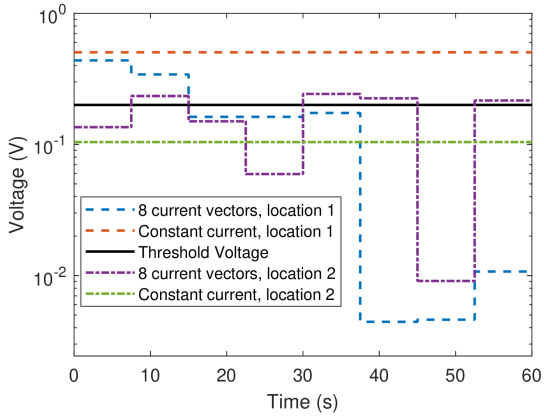

Fig. 6: Induced voltage in the receiver coil using 8 blind beamforming current vectors. Location 1 is the optimized position and location 2 is a randomly selected location.

also rotate the transmitting magnetic field's direction without considering the specific location of a receiver. Fundamentally, the two approaches are equivalent in the sense that the transmitter location can be considered as a special specific receiving location, where the beamforming vectors rotate.

IV. Numerical Simulations

In this section, we first evaluate the induced voltage and then we generate randomly orientated receiving coils and compare the reliability of different approaches. The employed values for the simulations are shown in Table II. Note that, the simulation in this section and the experiments in next section are conducted in the air. As shown in [12], the impact of soil is negligible when the distance between the transmitter and receiver is much smaller than the wavelength. The performance of wireless charging can be significantly affected by underground minerals. Nevertheless, most farming activities are conducted in shallow underground, where minerals are rare. If minerals exist on a farm, the deployment of sensor networks should consider it.

We compare MagBB with the constant current scenario, which has been used widely [8], [9]. In the constant current scenario, the current in each unidirectional coil is optimized to generate sufficient voltage/power at the receiver. However, the currents do not change and the magnetic field direction at the receiver is fixed. On the contrary, MagBB employs a set of optimized current vectors, which can generate different magnetic field directions at the receiver to ensure that part of the current vectors can efficiently charge the receiver.

A. Comparison of Induced Voltage

We test the performance of this system using a current set optimized for randomly oriented coil at a predetermined

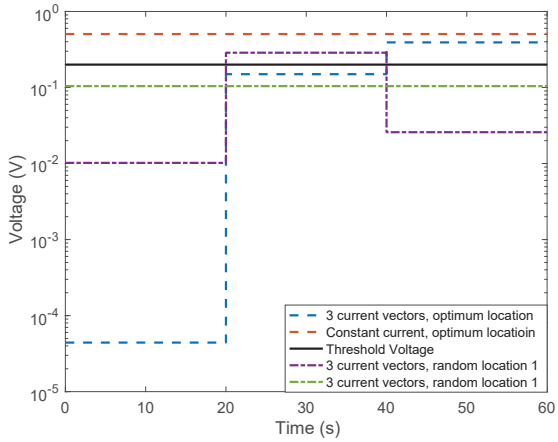

Fig. 7: Induced voltage in the receiver coil using 3 orthogonal blind beamforming current vectors. Location 1 is the optimized position and location 2 is a randomly selected location.

location with 1.0 m directly below the transmitter ($\theta_l = 180°$, $\phi_l = 0°$), which is the "location 1" in Fig. 6 and Fig. 7. Also, we compared with another location at ($\theta_l = 99.1°$, $\phi_l = 254.9°$), which is called "location 2" in Fig. 6 and Fig. 7. This location is randomly selected as an example. We then rotated the various coil orientations throughout the spherical region in predetermined steps and calculate the corresponding current values based on the optimization method outlined in Algorithm 1. We compare the induced voltage at a receiver placed at this location by the calculated optimal current vector to that of another coil at a different location. Lastly, we employ a simplistic approach by finding the maximum balanced current without exceeding the power threshold. We calculate the induced voltage at the predetermined locations and compared these with the results of the optimal current sets. Since the circuitry can be configured to invert negative voltages, the working range of the sensor consists of all induced voltages v_i such that $|v_i| > V_{th}$. We compare the voltage induced within a 60 s charging cycle.

Two optimized current sets with 3 and 8 current vectors are used. To test the efficacy of these current sets, we find the voltage induced for randomly located and oriented coils at a distance of 1.0 m from the transmitter by charging the receiver coils for an equal amount of time. We also use the simplistic approach by supplying the maximum allowable current to the transmitter coils per the power requirements specified for this system. i.e.,

$$\boldsymbol{i} = \sqrt{\frac{2P_{\max}}{3r_t}}[1,1,1]^T. \tag{38}$$

In this way, the transmission power is equally allocated to each transmit unidirectional coil and the currents are constants. The transmit coil number of turns is 50 and the receive coil number of turns is 10. The performance of the optimized and simplistic approaches in charging multiple randomly located and oriented receivers is compared in Fig. 6 and Fig. 7. The optimized current vectors show a clear advantage here as it is able to charge both receivers above the threshold voltage at certain points within the charging cycle. The constant current, however, either works throughout the charging cycle

(location 1) or does not charge the receiver at all throughout the charging cycle (location 2). This, therefore, makes the simplistic approach suboptimal for simultaneous charging at multiple locations.

However, this advantage comes with a heavy computation burden given the higher number of steps required. We explore the necessity and possibility of reducing this computational burden by producing a set of current vectors optimized for three mutually orthogonal coil orientations which are then tested in comparison with the constant current sets for the same locations. In order to observe the performance of the system with a minimum number of current values, we determine the orthonormal bases of 3 randomly generated unit currents. The optimum current values are then found for each orientation using the Algorithm 1. The performance is observed as shown in Fig. 7. As we can see, the 3 orthogonal current vectors can also achieve high induced voltage. Also, it provides more directional diversity compared with the constant current. Comparing Fig. 6 and Fig. 7, the 8-current set appears to charge the receiver more continuously given the higher resolution afforded by more current sets and more continuous rotation in the 3D space.

B. Reliability Evaluation

We then analyze the performance of the various current vectors for fixed locations at 0.5 m and at 1.0 m. We implicitly assume that the battery-free sensor has unlimited energy storage and in the following figures we show all the available received energy. We use 10,000 randomly positioned receivers and assume the receivers are only charged when the induced voltage is above the threshold voltage. The receiving coils are randomly orientated by letting their axes point to a random point on a unit hemisphere. The θ_r and ϕ_r for current vectors are obtained by uniformly sample points on a unit hemisphere at the receiver's location. In order to ensure that the magnetic field covers as much of a 3D space, the locations are chosen, based on which optimized currents are calculated, should be evenly spread out in space. Then, we calculate the received energy during one charging cycle. To make a fair comparison, we consider one cycle as 60 s, and a current vector uses $60/n_{cv}$ s. Then, we obtain the CDFs (Cumulative Distribution Function) for various policies and compare their performances.

First, in Fig. 8 and Fig. 9, we fix the receiver location and randomly generate its orientation. We use 8, 16, and 32 current vectors. As we can see, the constant currents always perform worse. By using the constant currents, some of the sensors that are aligned with the transmitter receive extremely high energy, while some of the sensors that are misaligned with the transmitter receive nearly zero energy. Thus, the received energy by sensors demonstrates a large variance. For example, at 1.0 m, by using the constant current vector, around 40% of the receivers cannot be charged at all. MagBB with rotating current vectors obtains a smaller variance and the percentage of uncharged sensors decreases to nearly zero. When the distance is 0.5 m, the three settings obtain similar performance. When the distance is small, the misalignment

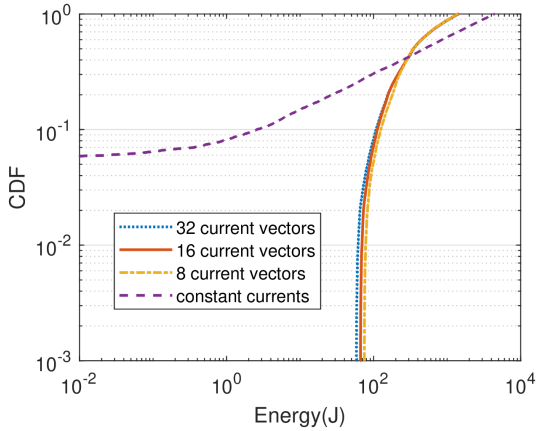

Fig. 8: CDF using 8, 16, and 32 blind beamforming current vectors at a fixed location ($\theta_l = 180°$, $\phi_l = 0°$) with a distance of 0.5 m.

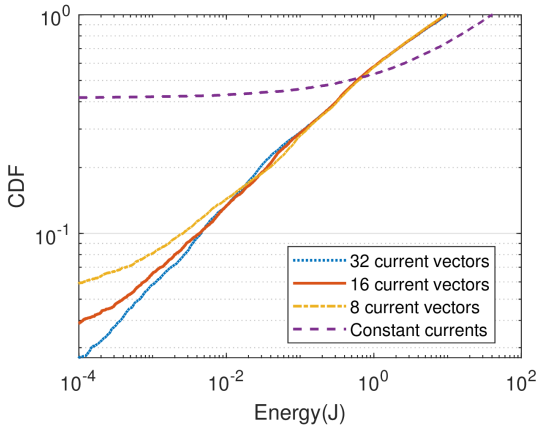

Fig. 9: CDF using 8, 16, and 32 blind beamforming current vectors at a fixed location ($\theta_l = 180°$, $\phi_l = 0°$) with a distance of 1.0 m.

loss can be compensated by the strong received voltage. Thus, the difference is small. However, as the distance increases to 1.0 m, the 32 current vectors demonstrate a small variance and the received energy by sensors is more homogeneous. Also, we notice that the received energy decreases dramatically as the distance increases. This is due to the small size of the receiving coil. Since the battery-free sensors have low power consumption, the harvested energy at the level of 1 mJ can be sufficient. Also, the charging time can be increased to meet the requirement of high-power-consumption sensors.

In Fig. 10 and Fig. 11, we vary both the receiver location and coil orientation. Our comparison suggests that there is about 40% probability that a randomly oriented coil is not charged at all by a constant current compared to about 2% for the 8 current vectors at 1.0 m. The performance gains achieved by using the optimized current sets are more pronounced at 1.0 m than at 0.5 m. An 8-current set is more computationally light and produces similar performance at 0.5 m, however, its performance deteriorates rapidly as the distance increases.

To evaluate the performance of the minimum number of current vectors, i.e., 3 current vectors, in Fig. 12 we show the CDF of the received energy. Comparing with the results in Fig. 12 and Fig. 11, the probability of receiving zero energy

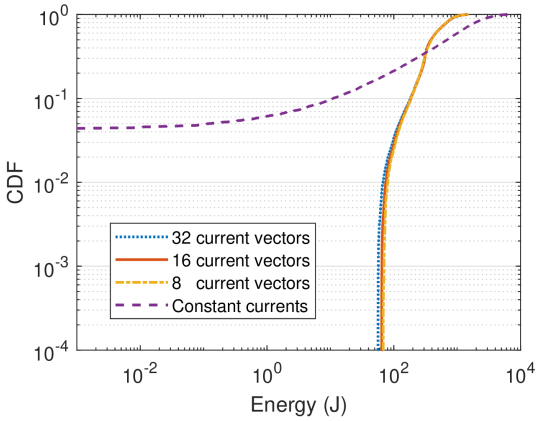

Fig. 10: CDF using 8, 16, and 32 blind beamforming current vectors for receive coils at random locations with random orientations. The receive coils are located on a sphere with radius of 0.5 m and the transmitter is in the center of the sphere.

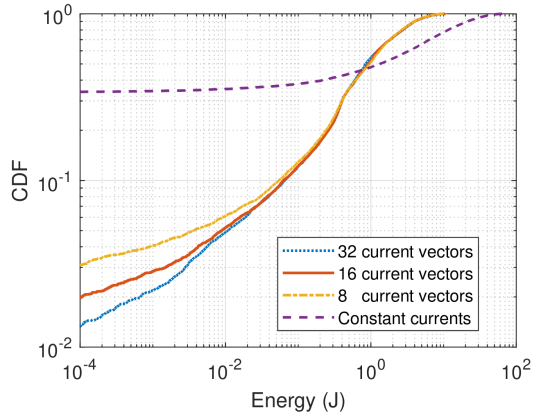

Fig. 11: CDF using 8, 16, and 32 blind beamforming current vectors for receive coils at random locations with random orientations. The receive coils are located on a sphere with radius of 1.0 m and the transmitter is in the center of the sphere.

at 1.0 m is lower than using constant current but higher than using 8 or more current vectors. At 0.5 m, the performance is similar to using more current vectors. Thus, if the wireless energy transfer range is long, i.e., around 1 m, it is more reliable to use more than 8 current vectors. On the contrary, if the range is short, i.e., around 0.5 m, it is sufficient to use 3 current vectors.

It should be noted that given the number of current vectors, we can optimally find the currents. This only needs to be calculated once. We can reuse the results without performing any online computation.

V. Proof-of-Concept Implementation

A. Prototype Design

In this section, we develop a proof-of-concept prototype, which is shown in Fig. 13 and Fig. 14. The prototype consists of a transmitter and a receiver. The tri-axis coil in the transmitter is made of three square unidirectional coils with 12 cm edge

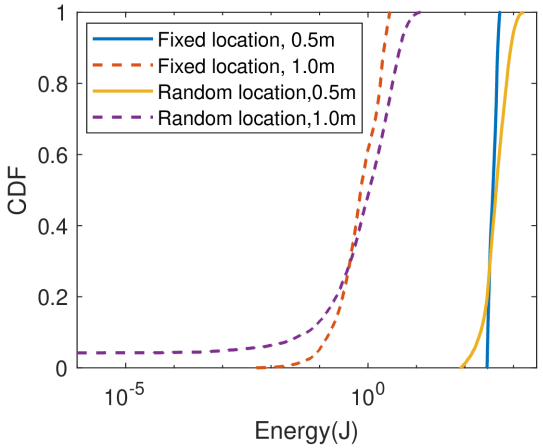

Fig. 12: CDF showing the performance of current vectors optimized for 3 mutually orthogonal receiver orientations at 0.5 m and 1.0 m radial distance.

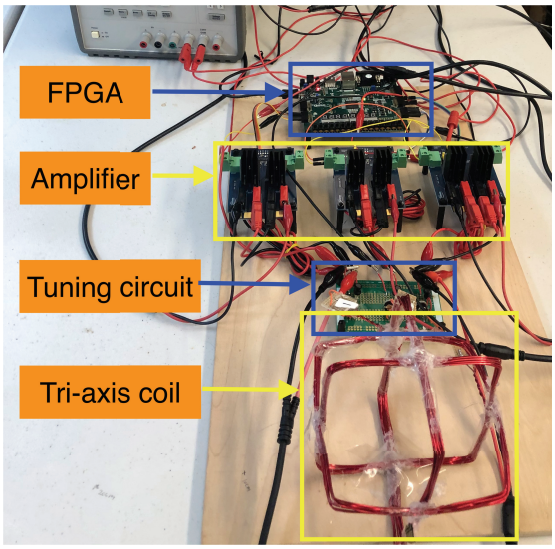

Fig. 13: The developed proof-of-concept prototype.

and 9 turns AWG 18 copper wire. The differences between the circular and square coils are compared in [39], which are small when coils are small compared with the wavelength. Since the coils are hand-made, they have slightly different mutual inductance (their mutual inductance are around 27 μH measured at 1 kHz). A matching circuit using a variable capacitor and 1.6 μH inductor is used to tune the output voltage.

Similar to the prototypes for wireless power transfer in [8], [10], [11], we use a MOSFET-based amplifier to control the output signal phase and amplitude. Since our considered output signal frequency is around 10 MHz, the switching frequency of the amplifier should support such a high frequency. We use three 2EDF7275F development boards from Infineon Technologies. The FPGA (Nexys4 FPGA board) is used to generate a controllable PWM wave to control the output of the amplifier. However, the output of the FPGA is 3.3 V which cannot support the original 2EDF7275F development board. We modified the board by reducing the resistor R38.

The Nexys4 FPGA board has an internal clock of 100 MHz.

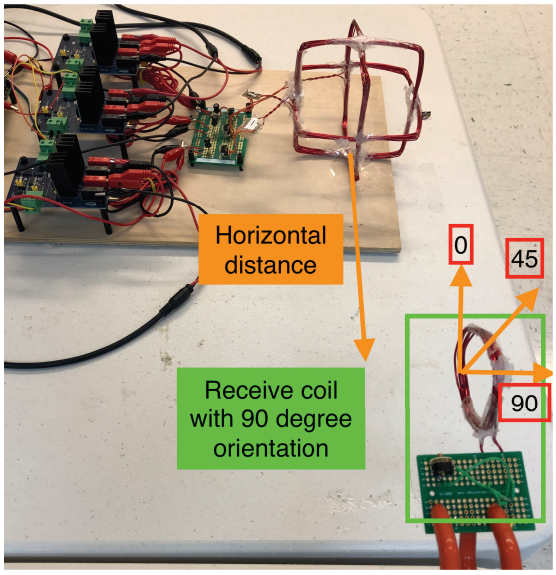

Fig. 14: Side view of the prototype and measurement setup. The receive coil is rotated with 0°, 45°, and 90° orientation.

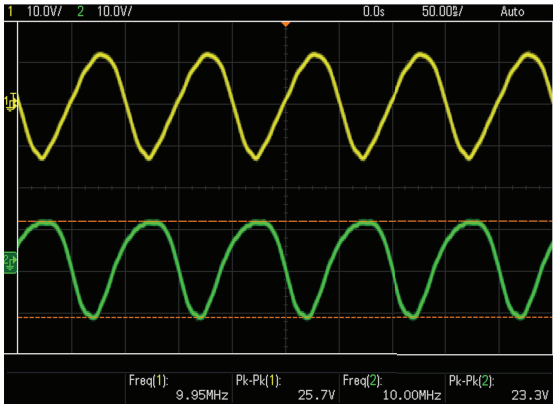

Fig. 15: Signals from the second and third coil with a 180° phase shift.

Instead of using 13.56 MHz, we generate signals at 10 MHz in the prototype. To control the magnitude of the output signal, we change the duty cycle of the PWM wave. Under a nearly matched condition, the impedance of a coil is mainly real resistance and, thus, the current is proportional to the voltage. By controlling the output voltage of the amplifier, we can control the currents in coils. In the near-field, magnetic fields do not propagate and the phase of the current vector is only 0° or 180°. We delay the PWM signal by a half cycle to generate 180° phase shift. An example of the output signal from the second and third unidirectional coil is shown in Fig. 15. As we can see from the figure, the voltage in the two coils has a phase shift of around 180°. Their magnitude are not exactly the same due to the imperfection of the coil.

Although theoretically the unidirectional coils are mutually perpendicular to each other and there is no coupling, in practice we notice there exists a reasonable coupling between unidirectional coils. For example, if we turn off the first and the second coil and turn on the third coil when the voltage in the third coil is around 23 V, we observe induced voltage in the first and second coil of around 8 V. This is due to two reasons.

TABLE III: Current Vectors

vectors	constant	1	2	3	4	5	6	7
coil 1	1	2	0	0	1	1	0	-1
coil 2	1	0	2	0	1	0	1	1
coil 3	1	0	0	2	0	1	1	0

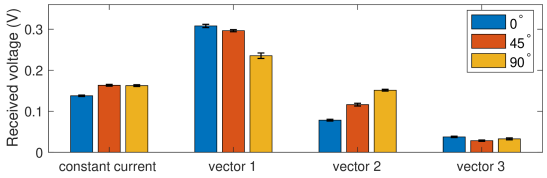

Fig. 16: Induced voltage in the receive coil with constant transmit current and three orthogonal currents.

First, the unidirectional coils are not exactly infinitesimal magnetic dipoles, which is an important assumption in our theoretical part. The multi-turn structure creates additional coupling between coils. Also, due to the high frequency, the cable also generates interference. We anticipate that using a more integrated circuit board and machine-manufactured coils will reduce this coupling.

To measure the received voltage, we use a small coil, as shown in Fig. 14, with a 2.5 cm radius and 7 turns of AWG 18 wire. A tunable capacitor is connected in parallel with the coil and the peak-to-peak induced voltage is measured using an oscilloscope. The coil's orientation is varied from 0° to 90° with a 45° step, as shown in Fig. 14. Due to the limited clock frequency of the FPGA, we can only generate two different magnitudes, which are denoted by 1 and 2. As shown in Table III, we created 8 current vectors. The first one is the constant current vector where the three coils use the same magnitude and phase. The current vectors 2 to 4 are three mutually orthogonal current vectors. We cannot generate 8 vectors as that in the numerical simulation due to the low resolution of the magnitude. When we use the magnitude 1, the output power from the power supply (including the power supply for the 2EDF7275F chip and the power supply for the MOSFET) is around 2.5 W, while we use the magnitude 2, the output power is around 6.0 W. Also, during our experiment, we notice the power cables also create some signal leakage. We use metal plates to shield the circuits and only keep the tri-axis coil outside, which effectively reduces the signal leakage.

B. Performance Evaluation

In Fig. 16, we compare the received voltage using the constant current and three orthogonal current vectors (vector 2, 3, and 4 in Table III when the receiver is placed 20 cm away from the center of the transmitter. For each orientation, we measure 5 voltages and plot the mean and standard deviation. First, we observe that although misalignment can cause losses, it cannot be infinite as predicted by the theoretical model, i.e., the received voltage is not zero even when coils are perpendicular in orientation. This is due to the structure of the coil, which is not a perfect magnetic dipole. Second, by exciting different transmit unidirectional coils, the received voltage can be drastically different. Thus, only using one

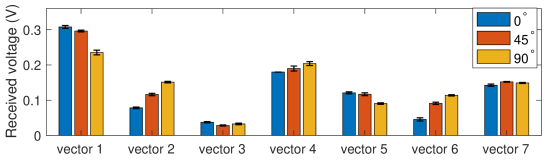

Fig. 17: Induced voltage in the receive coil with 7 current vectors.

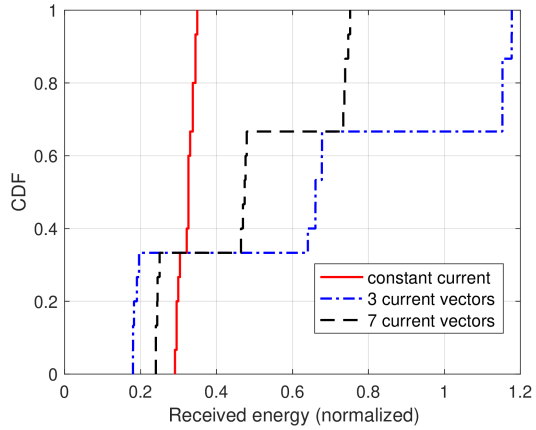

Fig. 18: CDF of normalized received energy at 10 cm away from the center of the transmit tri-axis coil using constant currents, three orthogonal current vectors (vectors 2, 3, and 4 in Table III), and 7 vectors (vectors 1 to 7 in Table III).

of the current vectors will result in inhomogeneous wireless charging. In Fig. 17, we show the received voltages for the current vectors 1 to 7. Similarly, these vectors also demonstrate a strong diversity, by rotating which we can ensure that some of these vectors generate high induced voltages.

To evaluate the reliability of using magnetic blind beamforming, we use the normalized received energy which is defined as $\sum_{i=1}^{n_{cv}} v_i^2/n_{cv}$. For a current vector, the received power is v_i^2 for a unit resister and the allocated time is $1/n_{cv}$. The v_i is collected using the same setting as previous discussions. We consider any voltages can be used since the receiver does not have a threshold voltage in our experiment setting (we use an oscilloscope to measured the received peak-to-peak voltage). As shown in Fig. 18, the constant current setting receives the minimum energy. The 7 current vectors perform worse than the 3 orthogonal current vectors. This is mainly due to the inhomogeneity of the transmission power. Since some of the 7 current vectors only use around 5 W transmission power, which is lower than that of the 3 orthogonal current vectors (around 6 W). Also, we observe that the 7 current vectors achieve a smaller variance than the 3 orthogonal current vectors. This is also observed in Fig. 19 when the transmitter and the receiver are separated by 20 cm. In Fig. 19, the constant current setting demonstrates a large variance and small received energy.

In the prototype, we can obtain a range of 30 cm with above 100 mV induced voltage. However, as the distance increases, the induced voltage drops below 100 mV. Since the proposed application is for wireless charging for underground sensors, we can further increase the transmission power. Also, by using more integrated circuits and perfectly matched coils,

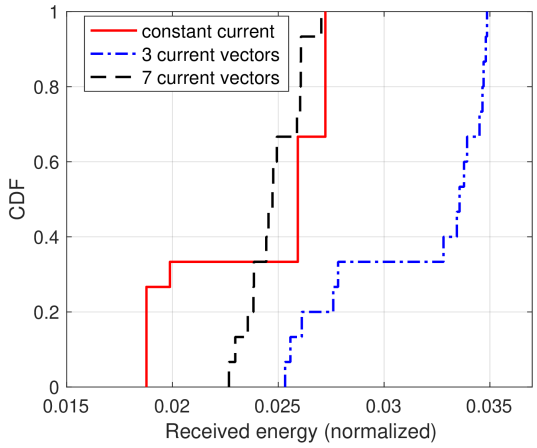

Fig. 19: CDF of normalized received energy at 20 cm away from the center of the transmit tri-axis coil using constant currents, three orthogonal current vectors (vectors 2, 3, and 4 in Table III), and 7 vectors (vectors 1 to 7 in Table III).

the efficiency can be further improved.

C. Limitations and Future Work

MagBB can only be used for short-range battery-free sensor networks due to the following limitations. First, it is challenging to obtain a range beyond 2 m due to the small coil size. Since the envisioned application is for ultra-dense IoT, the size of sensor coil is small; the coil is not efficient in receiving power. Moreover, since magnetic fields decrease in 30 dB/decade in the near-field, simply increasing transmission power cannot guarantee a long operation range. Second, the current proof-of-concept prototype experiences coil mutual coupling, electromagnetic noises, and limited magnitude control. It can be improved using precise calibration of coils and a high-end FPGA with a faster clock. The precise calibration of coils can reduce mutual coupling. Also, a faster FPGA will allow us to generate more magnitudes. The prototype can be better shielded to reduce electromagnetic interferences and noises. This can potentially further increase the operation range. The future work of this paper will focus on improving the efficiency of the prototype by calibrating the coils and considering electromagnetic compatibility. Also, the model can be improved by considering imperfect coils, such as the coil mutual coupling.

VI. CONCLUSION

A magnetic blind beamforming (MagBB) algorithm using tri-axis coils is proposed in this paper to wirelessly charge battery-free sensors with unknown coil orientations and locations. The efficiency of magnetic signal-based wireless energy transfer strongly depends on the coil alignment. The misalignment causes significant losses. Since battery-free sensors use diodes in the energy harvesting circuit, if the induced voltage is lower than the diode threshold voltage, no energy can be received. MagBB can rotate magnetic fields at a point that can ensure that a part of the magnetic fields can be leveraged to charge a sensor. This paper provides a detailed design procedure for MagBB and discusses its reliability,

location dependency, and efficiency. Extensive simulations are performed to evaluate the performance of MagBB. A proof-of-concept prototype is developed to verify the performance of MagBB. The results suggest that MagBB can effectively charge sensors without knowing their coil orientation.

REFERENCES

[1] A. A. Ofori and H. Guo, "MagBB: Wireless Charging for Batteryless Sensors Using Magnetic Blind Beamforming," in *2021 IEEE 18th Annual Consumer Communications & Networking Conference (CCNC)*. IEEE, 2021, pp. 1–8.

[2] X. Dong, M. C. Vuran, and S. Irmak, "Autonomous precision agriculture through integration of wireless underground sensor networks with center pivot irrigation systems," *Ad Hoc Networks*, vol. 11, no. 7, pp. 1975–1987, 2013.

[3] M. C. Vuran, A. Salam, R. Wong, and S. Irmak, "Internet of underground things in precision agriculture: Architecture and technology aspects," *Ad Hoc Networks*, vol. 81, pp. 160–173, 2018.

[4] G. Maselli, M. Pietrogiacomi, M. Piva, and J. A. Stankovic, "Battery-free smart objects based on rfid backscattering," *IEEE Internet of Things Magazine*, vol. 2, no. 3, pp. 32–36, 2019.

[5] Y. Ma, Z. Luo, C. Steiger, G. Traverso, and F. Adib, "Enabling deep-tissue networking for miniature medical devices," in *Proceedings of the 2018 Conference of the ACM Special Interest Group on Data Communication*, ser. SIGCOMM '18. New York, NY, USA: Association for Computing Machinery, 2018, p. 417–431.

[6] S. N. Daskalakis, G. Goussetis, and A. Georgiadis, "Nfc hybrid harvester for battery-free agricultural sensor nodes," in *2019 IEEE International Conference on RFID Technology and Applications (RFID-TA)*. IEEE, 2019, pp. 22–25.

[7] K. Geissdoerfer and M. Zimmerling, "Bootstrapping battery-free wireless networks: Efficient neighbor discovery and synchronization in the face of intermittency." in *NSDI*, 2021, pp. 439–455.

[8] J. Jadidian and D. Katabi, "Magnetic MIMO: How to charge your phone in your pocket," in *Proceedings of the 20th annual international conference on Mobile computing and networking*, 2014, pp. 495–506.

[9] G. Yang, M. R. V. Moghadam, and R. Zhang, "Magnetic mimo signal processing and optimization for wireless power transfer," *IEEE Transactions on Signal Processing*, vol. 65, no. 11, pp. 2860–2874, 2017.

[10] L. Shi, Z. Kabelac, D. Katabi, and D. Perreault, "Wireless power hotspot that charges all of your devices," in *Proceedings of the 21st Annual International Conference on Mobile Computing and Networking*, 2015, pp. 2–13.

[11] G. Cao, H. Zhou, H. Zhang, J. Xu, P. Yang, and X.-Y. Li, "Requirement-driven magnetic beamforming for mimo wireless power transfer optimization," in *2018 15th Annual IEEE International Conference on Sensing, Communication, and Networking (SECON)*. IEEE, 2018, pp. 1–9.

[12] H. Guo and A. A. Ofori, "The internet of things in extreme environments using low-power long-range near field communication," *IEEE Internet of Things Magazine*, vol. 4, no. 1, pp. 34–38, 2021.

[13] X. Liu and N. Ansari, "Toward green iot: Energy solutions and key challenges," *IEEE Communications Magazine*, vol. 57, no. 3, pp. 104–110, 2019.

[14] P. Zhou, C. Wang, and Y. Yang, "Design of self-sustainable wireless sensor networks with energy harvesting and wireless charging," *ACM Transactions on Sensor Networks (TOSN)*, vol. 17, no. 4, pp. 1–38, 2021.

[15] T. Sasatani, C. J. Yang, M. J. Chabalko, Y. Kawahara, and A. P. Sample, "Room-wide wireless charging and load-modulation communication via quasistatic cavity resonance," *Proceedings of the ACM on Interactive, Mobile, Wearable and Ubiquitous Technologies*, vol. 2, no. 4, pp. 1–23, 2018.

[16] K. Sumiya, T. Sasatani, Y. Nishizawa, K. Tsushio, Y. Narusue, and Y. Kawahara, "Alvus: A reconfigurable 2-d wireless charging system," *Proceedings of the ACM on Interactive, Mobile, Wearable and Ubiquitous Technologies*, vol. 3, no. 2, pp. 1–29, 2019.

[17] Z. Sun and I. F. Akyildiz, "Magnetic induction communications for wireless underground sensor networks," *IEEE transactions on antennas and propagation*, vol. 58, no. 7, pp. 2426–2435, 2010.

[18] H. Zhou, Z. Chen, W. Zhou, H. Tan, P. Yang, and X.-Y. Li, "Camel: Context-aware magnetic mimo wireless power transfer with in-band communication," in *IEEE INFOCOM 2021-IEEE Conference on Computer Communications*. IEEE, 2021, pp. 1–10.

[19] M. R. V. Moghadam and R. Zhang, "Node placement and distributed magnetic beamforming optimization for wireless power transfer," *IEEE Transactions on Signal and Information Processing over Networks*, vol. 4, no. 2, pp. 264–279, 2017.

[20] Y. Zhang, D. Chen, and T. Jiang, "Robust beamforming design for magnetic mimo wireless power transfer systems," *IEEE Transactions on Signal Processing*, vol. 69, pp. 5066–5077, 2021.

[21] H. Zhou, J. Deng, W. Hua, X. Cui, X.-Y. Li, and P. Yang, "Procs: Power routing and current scheduling in multi-relay magnetic mimo wpt system," *IEEE Transactions on Mobile Computing*, 2021.

[22] W. Zhou, H. Zhou, W. Hua, F. Zhou, X. Cui, S. Tang, Z. Liu, and X.-Y. Li, "Imp: Impedance matching enhanced power-delivered-to-load optimization for magnetic mimo wireless power transfer system," in *2021 IEEE/ACM 29th International Symposium on Quality of Service (IWQOS)*. IEEE, 2021, pp. 1–10.

[23] R. Lin, H.-J. Kim, S. Achavananthadith, S. A. Kurt, S. C. Tan, H. Yao, B. C. Tee, J. K. Lee, and J. S. Ho, "Wireless battery-free body sensor networks using near-field-enabled clothing," *Nature communications*, vol. 11, no. 1, pp. 1–10, 2020.

[24] J. Wang, J. Zhang, K. Li, C. Pan, C. Majidi, and S. Kumar, "Locating everyday objects using nfc textiles," in *Proceedings of the 20th International Conference on Information Processing in Sensor Networks (co-located with CPS-IoT Week 2021)*, 2021, pp. 15–30.

[25] L. Li, H. Dai, G. Chen, J. Zheng, W. Dou, and X. Wu, "Radiation constrained fair charging for wireless power transfer," *ACM Transactions on Sensor Networks (TOSN)*, vol. 15, no. 2, pp. 1–33, 2019.

[26] Y. Ma, W. Liang, and W. Xu, "Charging utility maximization in wireless rechargeable sensor networks by charging multiple sensors simultaneously," *IEEE/ACM Transactions on Networking*, vol. 26, no. 4, pp. 1591–1604, 2018.

[27] A. Markham and N. Trigoni, "Magneto-inductive networked rescue system (miners) taking sensor networks underground," in *Proceedings of the 11th international conference on Information Processing in Sensor Networks*, 2012, pp. 317–328.

[28] Z. Zhang, E. Liu, X. Qu, R. Wang, H. Ma, and Z. Sun, "Connectivity of magnetic induction-based ad hoc networks," *IEEE Transactions on Wireless Communications*, vol. 16, no. 7, pp. 4181–4191, 2017.

[29] S. Kisseleff, I. F. Akyildiz, and W. Gerstacker, "Beamforming for magnetic induction based wireless power transfer systems with multiple receivers," in *2015 IEEE Global Communications Conference (GLOBECOM)*. IEEE, 2015, pp. 1–7.

[30] H. Guo, Z. Sun, and P. Wang, "Joint design of communication, wireless energy transfer, and control for swarm autonomous underwater vehicles," *IEEE Transactions on Vehicular Technology*, vol. 70, no. 2, pp. 1821–1835, 2021.

[31] S. P. Ravindran, J.-F. Bousquet, and N. Gaoding, "Characterization of a 3d underwater magneto-inductive transmitter coil array," in *OCEANS 2018 MTS/IEEE Charleston*. IEEE, 2018, pp. 1–6.

[32] C. A. Balanis, *Antenna theory: analysis and design*. John wiley & sons, 2016.

[33] W. C. Chew, *Waves and fields in inhomogeneous media*. IEEE press, 1995.

[34] Z. Luo, W. Ma, A. M. So, Y. Ye, and S. Zhang, "Semidefinite relaxation of quadratic optimization problems," *IEEE Signal Processing Magazine*, vol. 27, no. 3, pp. 20–34, 2010.

[35] M. Grant and S. Boyd, "CVX: Matlab software for disciplined convex programming, version 2.1," http://cvxr.com/cvx, Mar. 2014.

[36] ——, "Graph implementations for nonsmooth convex programs," in *Recent Advances in Learning and Control*, ser. Lecture Notes in Control and Information Sciences, V. Blondel, S. Boyd, and H. Kimura, Eds. Springer-Verlag Limited, 2008, pp. 95–110, http://stanford.edu/~boyd/graph_dcp.html.

[37] C. Helmberg, F. Rendl, R. J. Vanderbei, and H. Wolkowicz, "An interior-point method for semidefinite programming," *SIAM Journal on optimization*, vol. 6, no. 2, pp. 342–361, 1996.

[38] W.-K. Ma, C.-C. Su, J. Jaldén, and C.-Y. Chi, "Some results on 16-qam mimo detection using semidefinite relaxation," in *2008 IEEE International Conference on Acoustics, Speech and Signal Processing*. IEEE, 2008, pp. 2673–2676.

[39] A. F. R. Alvarez, E. Franco-Mejia, and C. R. Pinedo-Jaramillo, "Study and analysis of magnetic field homogeneity of square and circular helmholtz coil pairs: A taylor series approximation," in *2012 VI Andean Region International Conference*. IEEE, 2012, pp. 77–80.

Albert Aninagyei Ofori received his Master's degree in Electronics Engineering at the Norfolk State University, Virginia in December 2021, and his Bachelor of Science degree in Electrical and Electronics Engineering at the Kwame Nkrumah University of Science and Technology, Ghana in July 2017. He has internship experience in software engineering at Amazon Web Services, Inc and Cirrus Logic, Inc. His research interests involve wireless communication and wireless power transfer.

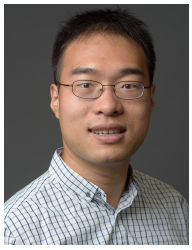

Hongzhi Guo received his Ph.D. degree from University at Buffalo, the State University of New York in 2017, and his MS degree from Columbia University in 2013, both in Electrical Engineering. Currently, he is an assistant professor in the Engineering Department at Norfolk State University. His broad research agenda is to develop the foundations for wireless sensor networks and networked robotics to automate dangerous, dirty, dull tasks in extreme environments, such as underground and underwater. He received the NSF CRII award in 2020, the Jeffress Trust Awards Program in Interdisciplinary Research in 2020, the NSF HBCU-UP RIA award in 2020, and the Best Demo Award in IEEE INFOCOM 2017.